

See discussions, stats, and author profiles for this publication at: <https://www.researchgate.net/publication/230891291>

# The Orbital Theory of Pleistocene Climate: Support from a Revised Chronology of the Marine d18O Record

Chapter · January 1984

CITATIONS

177

READS

185

9 authors, including:



J. D. Hays

Lamont - Doherty Earth Observatory Columb...

82 PUBLICATIONS 10,949 CITATIONS

SEE PROFILE



Douglas Martinson

Columbia University

101 PUBLICATIONS 12,858 CITATIONS

SEE PROFILE



Alan C. Mix

Oregon State University

333 PUBLICATIONS 14,637 CITATIONS

SEE PROFILE



Nicklas G. Pisias

Oregon State University

152 PUBLICATIONS 13,732 CITATIONS

SEE PROFILE

Some of the authors of this publication are also working on these related projects:



The Biological Pump During the Last Glacial Maximum and Early Deglaciation [View project](#)

THE ORBITAL THEORY OF PLEISTOCENE CLIMATE: SUPPORT FROM A REVI-  
SED CHRONOLOGY OF THE MARINE  $\delta^{18}\text{O}$  RECORD

J. Imbrie<sup>1,3</sup>, J.D. Hays<sup>3</sup>, D.G. Martinson<sup>5</sup>,  
A. McIntyre<sup>3</sup>, A.C. Mix<sup>3</sup>, J.J. Morley<sup>2</sup>, N.G. Pisias<sup>4</sup>,  
W.L. Prell<sup>1</sup>, and N.J. Shackleton

<sup>1</sup>Brown University, Providence, RI 02912, USA

<sup>2</sup>Cambridge University, Cambridge, England

<sup>3</sup>Lamont-Doherty Geological Observatory, Columbia  
University, Palisades, NY, USA

<sup>4</sup>Oregon State University, Corvallis, OR, USA

<sup>5</sup>Woods Hole Oceanographic Institution, Woods Hole,  
MA, USA

Observations of  $\delta^{18}\text{O}$  in five deep-sea cores provide a basis for developing a geological time scale for the past 780 000 years and for evaluating the orbital theory of Pleistocene ice ages. The isotopic measurements are obtained from shallow-dwelling planktonic foraminifera at widely distributed, open-ocean sites in low- and mid-latitudes. The amplitudes of oscillations in this homogeneous set of isotopic records are highly correlated and must be strongly influenced by changes in the global volume of glacial ice. Three of the cores studied penetrate the Brunhes-Matuyama magnetic reversal, an event previously dated by K-Ar measurements at 730 KY BP. This date, and the assumption that variations in orbital precession and obliquity cause changes in global climate, are used to develop a new time scale for the  $\delta^{18}\text{O}$  record. Displayed on this time scale, the isotopic variations are phase locked ( $\pm 15^\circ$ ) and strongly coherent ( $> 0.9$ ) with orbital variations --not only at the main periods of precession (19 KY and 23 KY) and obliquity (41 KY), but also in the 100-KY eccentricity band. This statistical evidence of a close relationship between the time-varying amplitudes of orbital forcing and the time-varying amplitudes of the isotopic response implies that orbital variations are the main external cause of the succession of late Pleistocene ice ages.

## INTRODUCTION

Since the pioneer work of James Croll (1864-1875) and Milutin Milankovitch (1920-1941), the central geological problem in testing the astronomical theory of the Pleistocene ice ages has been the difficulty of obtaining a chronology of climatic events that was sufficiently accurate to serve this purpose yet sufficiently independent of the theory itself to make the test credible (5,21,39). The advent of deep-sea piston coring in 1947 (40) opened the way for a fresh attack on this problem by providing sedimentary records of climate that were deposited at relatively constant rates over intervals of time long enough to be relevant to the astronomical theory. Paramount among such records are curves showing fluctuations in the ratio of  $^{18}\text{O}$  to  $^{16}\text{O}$  in tests of fossil foraminifera. These curves monitor major changes in global climate as the Earth shifts towards or away from an ice-age condition -- an approach to climate history that was pioneered in 1955 by Emiliani (8).

In the present study we analyze isotopic data from five deep-sea cores. Three of these penetrate the Brunhes-Matuyama magnetic reversal, an event dated radiometrically at 730 KY BP. We use this datum, as well as certain assumptions about the astronomical control of Pleistocene climate, to develop a time scale for the isotopic record. Finally, we present evidence that our chronology is sufficiently accurate to permit a meaningful evaluation of the Milankovitch theory.

The  $^{18}\text{O}$  Record

Measurements of the ratio of  $^{18}\text{O}$  to  $^{16}\text{O}$  are reported with respect to an international standard as  $\delta^{18}\text{O}$  in parts per thousand (‰). In his initial study, Emiliani (8) argued that the dominant cause of Pleistocene  $\delta^{18}\text{O}$  variations is a change in ambient water temperature. Later work by Olausson (23), by Shackleton (28) and by Shackleton and Opdyke (32) led to the conclusion now generally accepted that downcore variations in  $\delta^{18}\text{O}$  reflect changes in oceanic isotopic composition, and that these changes are caused primarily by the waxing and waning of the great Pleistocene ice sheets. Fairbanks and Matthews (10), for example, estimate that 0.011 per mil of  $\delta^{18}\text{O}$  variation is associated with 1 m of sea-level change. Subsequent work (6,7) has emphasized that a number of influences (in addition to variations in global ice volume) may have a significant effect on the shape of particular  $\delta^{18}\text{O}$  curves. These influences include: (1) changes in ambient water temperature; (2) changes in the evaporation-precipitation ratio at the site of formation of the water mass under study; (3) vital and ecological effects of individual species; (4) differential dissolution; (5) sediment transport; (6) bioturbation; and (7) stratigraphic distur-

bance. With these influences in mind, we have designed a sampling strategy that will enhance the effect of ice-volume variations and suppress the effect of other influences.

### Sampling Strategy

First, we choose cores from open-ocean sites in low- and mid-latitudes that accumulated relatively rapidly and at depths relatively unaffected by dissolution (Fig. 1, Table 1). Second, we limit our study to shallow-dwelling planktonic species. Four of our records are based on Globigerinoides sacculifer. One record (RC11-120) is based on Globigerina bulloides. Finally, after analyzing each core individually, we normalize and average the records to produce a stacked record in which most of the influences other than ice-volume will tend to cancel each other out. The benefits of stacking noisy, individual  $\delta^{18}\text{O}$  records were recognized by Emiliani (9), who recast his observations in the form of a generalized isotopic curve.

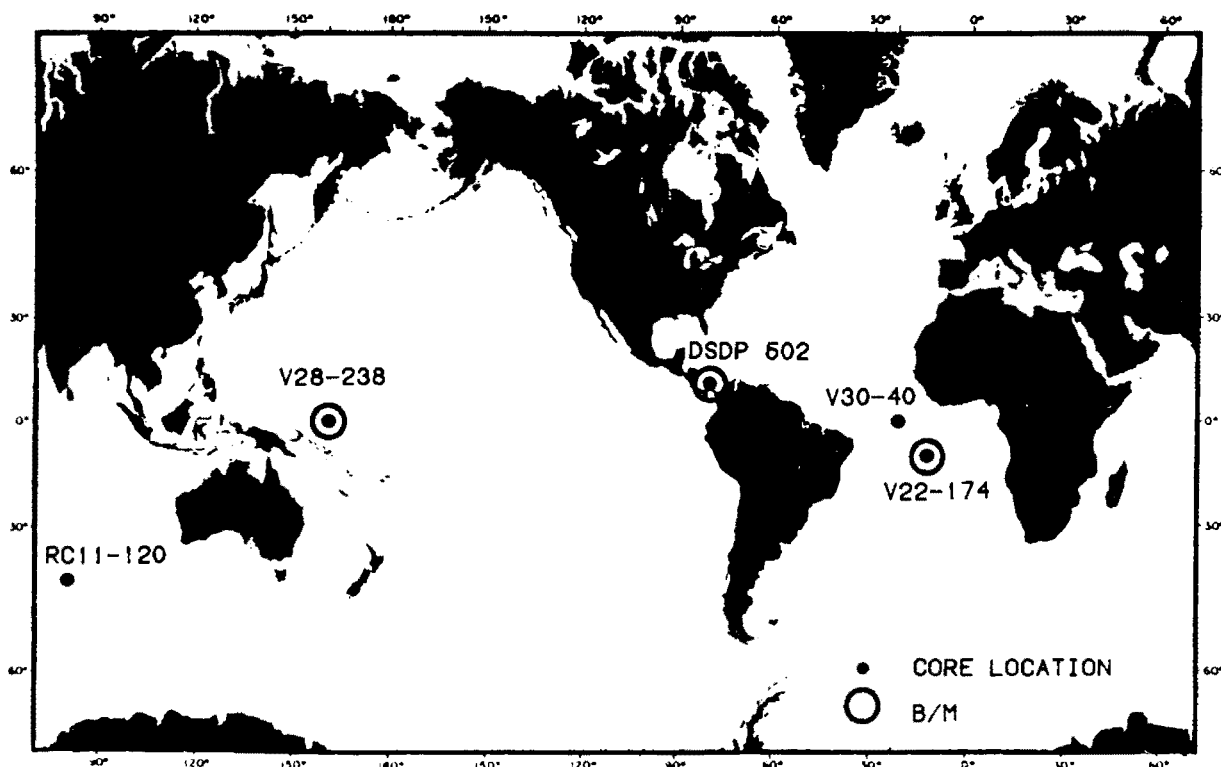


Figure 1 Location of cores used in this study. The symbol B/M indicates a core that penetrates the Brunhes-Matuyama magnetic reversal.

### Standard Isotopic Stratigraphy

Like all stratigraphic records,  $\delta^{18}\text{O}$  curves are subject to distortion by vagaries of the depositional process. Other dis-

Table 1 Location and description of cores.

Core	Ref.	Lat.	Long.	Water Depth (M)	Core Length (CM)	Ave. Acc. Rate (CM/KY)	Ave. Sampling Interval (KY)
RC11-120	(13)	43°31'S	79°52'E	3193	954	3.3	1.5
V22-174	(36)	10°04'S	12°49'W	2630	1566	1.9	4.8
V30-40	(42)	00°12'S	23°09'W	3706	755	2.8	1.1
V28-238	(30,32)	01°01'N	160°29'E	3120	1609	1.6	5.0
DSDP502b	(26)	11°30'N	79°23'W	3051	3584	2.2	4.7

tortions may result from the coring process itself. In order to identify and allow for such distortions before developing our time scale, we have made detailed comparisons between the isotopic events recorded in each core with events recorded in other cores. Toward this end, we have made extensive use of a stratigraphic study of a global set of  $\delta^{18}\text{O}$  records conducted as part of the SPECMAP project (27). In essence, this study is an extension (9,29,32,33) of the concept of numbered isotopic stages initiated by Emiliani (8). In Emiliani's scheme, stages are numbered consecutively from the top of the record downward, with odd numbered stages corresponding to interglacial (isotopically light) intervals and even numbers corresponding to glacial intervals. In most cases, stage boundaries correspond to rapid, monotonic shifts in the curve. This scheme has proved very useful in describing and analyzing climate history back through Stage 22. As a result, earlier papers dealing with  $\delta^{18}\text{O}$  chronology have presented their results in terms of stage boundaries. However, we consider that for purposes of detailed correlation this scheme should be supplemented by using the stratigraphic system proposed by Prell et al. (27).

The essential feature of this system is the identification of all negative and positive excursions (peaks and valleys) that are globally persistent. The stages previously defined are retained, and the isotopic events within stages are given a decimal notation such that negative (interglacial) and positive (glacial) excursions have odd and even numbers, respectively. For example, the negative events in Stage 5 previously called 5a, 5c, and 5e are designated 5.1, 5.3, and 5.5; the positive events previously called 5b and 5d are designated 5.2 and 5.4; and the boundary between Stage 5 and Stage 6 is designated 6.0. Clearly, this is a convenient and flexible notation. Our main reason for adopting it, however, is that the exact stratigraphic level of a peak or a valley can be defined unambiguously in one curve and recognized with a high degree of precision in another. This is often not true of stage boundaries. Most of the control points in our chronology have therefore been placed at the extremes of excursions recognized and numbered by Prell et al. (27).

## A NEW LATE-PLEISTOCENE $\delta^{18}\text{O}$ CHRONOLOGY

### Previous Work

Several recently published  $\delta^{18}\text{O}$  chronologies have been based on a combination of radiometric control and astronomic theory (13,17,18,22). Broadly speaking, the results of these investigations are concordant over the past 400 KY, but discordant from 400 KY to 800 KY BP. Important discrepancies occur at

the Brunhes-Matuyama boundary, dated radiometrically at  $730 \pm 11$  KY (20). In the time scales produced by Kominz et al. (18), Morley and Hays (22), and Johnson (17), this event is dated at 728 KY, 738 KY, and 790 KY, respectively. Some of these differences result from using different sets of basic data. However, most of them are the result of using different strategies to develop a time scale over a portion of the record for which only a small number of precise radiometric dates are available.

All of the studies cited above make an initial assumption that the sediment accumulation function (depth-in-core vs. age) is linear between radiometric control points. All then relax this assumption to produce a satisfactory match between the adjusted isotopic curve and one or more astronomical curves that have been designated as targets of the tuning procedure. As shown in Table 2, differences between one procedure and another can be described in terms of five elements of tuning strategy: (1) the choice of a target curve, i.e., an astronomical curve (or curves) assumed to represent the forcing function of the climate system; (2) an estimate of the phase lag between the assumed forcing function and the isotopic response; (3) the selection of a data processing technique to achieve a match between the astronomical and isotopic curves; (4) the number of control points allowed in the depth-vs.-age function; and (5) the criteria used to evaluate the postulated match between the astronomical and tuned isotopic curves.

#### A Revised Tuning Strategy

Target curves. Several investigators have used an insolation curve for a particular latitude and season as a tuning target. Instead, we follow Hays et al. (13) and Morley and Hays (22) by matching isotopic observations against curves showing variations in obliquity ( $\epsilon$ ) and variations in the precession index ( $\Delta e \sin \omega$ ). This procedure has two significant benefits, one practical and one theoretical. On the practical side, the procedure is parsimonious: curves of  $\epsilon$  and  $\Delta e \sin \omega$  contain all of the information needed to calculate an insolation curve for any latitude and any season (2). In fact, to a high degree of accuracy, any insolation curve outside of the polar regions can be computed from these two orbital parameters by a simple linear transfer function involving only the ratio of the two parameters and the phase of  $\omega$ , the longitude of perihelion (14). Theoretical benefits follow because there is widespread agreement on the general (if not the detailed) nature of the physical mechanisms by which the climate system responds to insolation changes driven by variations in obliquity (at periods of 41 KY) and precession (at 19 KY and 23 KY). In contrast, there is little agreement on the nature of the physical mechanisms responsible for the climatic oscillations around 100 KY that dominate the isotopic record.

Table 2 Elements of different tuning strategies

Reference	Astronomical Target Curve(s)	Phase Lag of $\delta^{18}O$ Response	Data Processing	Number of Non-radiometric Control Points within the Brunhes	Independent Evaluation Criteria
Emiliani (1955)	45°N summer insolation	5 KY	raw data		
Hays et al. (1976)	obliquity precession	9 KY 3 KY	41 K filter 23 K filter	2	
Kominz et al. (1979)	obliquity	10 KY	41 K filter complex demodulation	12	23 K filter COH (f)
Morley and Hays (1981)	obliquity precession	90° 90°	raw data	17	19 K filter 23 K filter 41 K filter
Johnson (1982)	35°N and 70°N	5 KY?	raw data	15	
This paper	obliquity precession	- arctan 2 f(17 KY)	22 K filter 41 K filter	56-72	COH (f) depth vs. age



As shown by Berger (3) and displayed in Figure 2, the obliquity signal has a simple spectrum with variance concentrated near periods of 41 KY. The spectrum of the precession index (which we will hereafter refer to as precession) is more complex, with variance concentrated near periods of 19 KY and 23 KY. In principle, one could follow Morley and Hays (22) and tune the isotopic curve separately against the 19 KY and 23 KY components of precession (Fig. 3). However, the length of a digital filter required to achieve the necessary resolution makes this strategy undesirable.

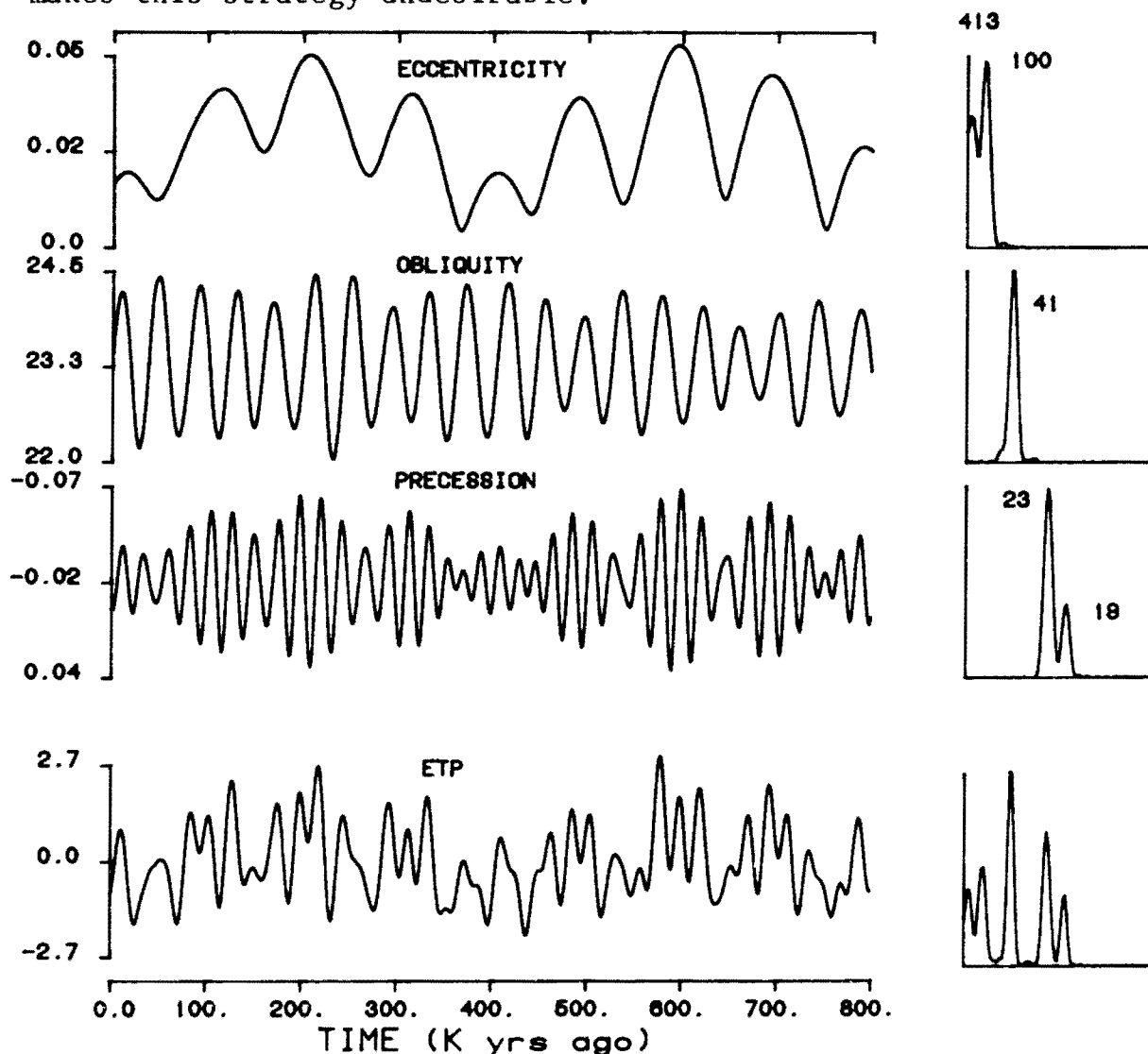


Figure 2 Variations in eccentricity, obliquity, and the precession index ( $\Delta e \sin \omega$ ) over the past 800 000 years. Left: The three upper time series are from the work of Berger (1). These have been normalized and added to form the curve labeled ETP. The scale for obliquity is in degrees; for ETP, in standard deviation units. Right: Variance spectra calculated from these time series, with the dominant periods (KY) of conspicuous peaks indicated.

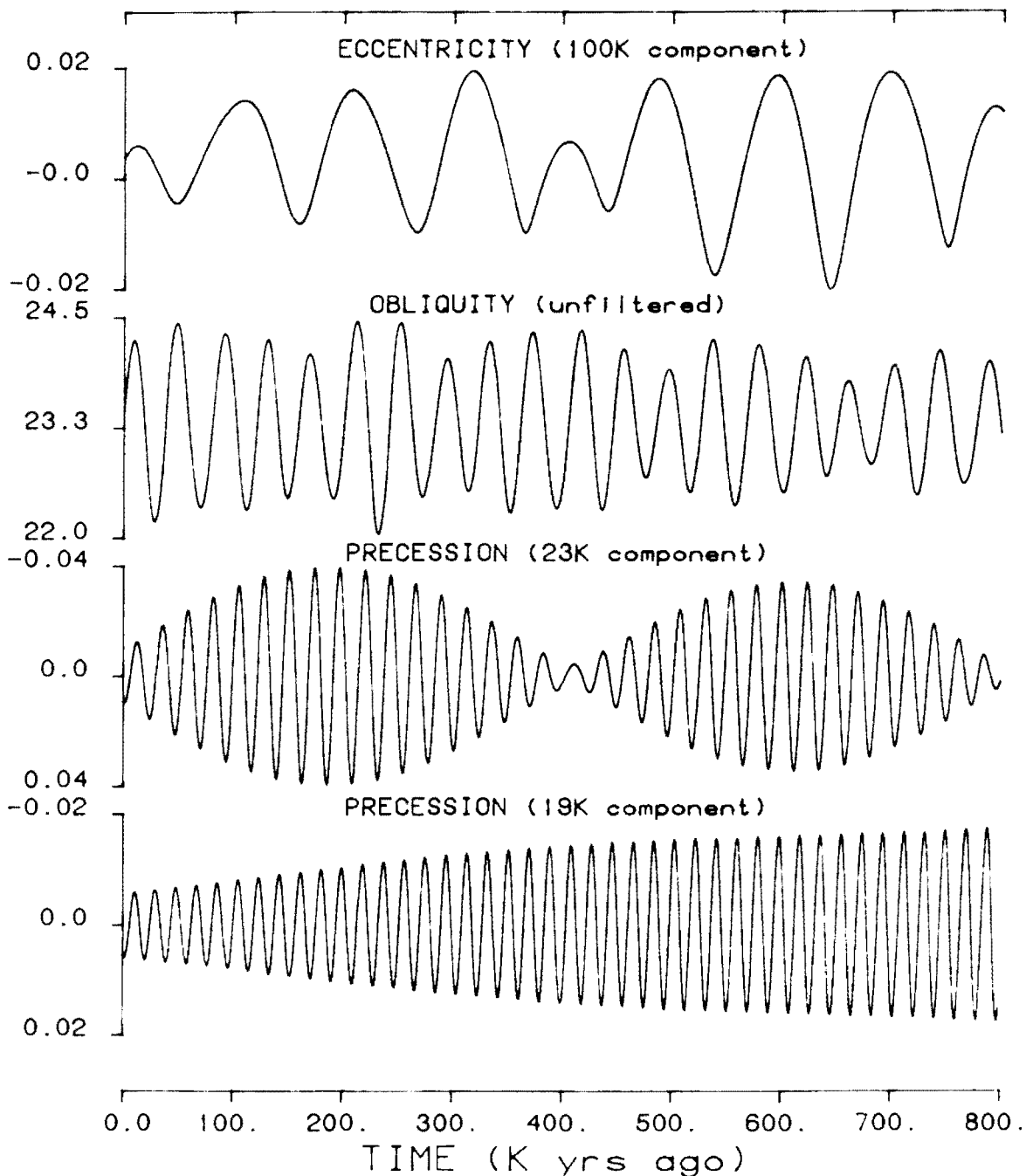


Figure 3 Narrow-band variations in eccentricity, obliquity, and the precession index ( $\Delta e \sin \omega$ ) over the past 800 000 years. The top curve consists of components of eccentricity variation having periods near 100 KY, and was obtained by digital filtering. Curves showing the 19 KY and 23 KY components of the precession index are obtained in the same way. The obliquity curve has not been filtered. Calculations made by the authors on primary orbital curves provided by A.L. Berger (1).

Phase Lag. Based on Weertman's ice-sheet model (38), the mean time constant of large ice sheets (expressed as an e-folding time) can be estimated to lie in the range 10 KY to 20 KY. Because these values are of the same order of magnitude as the periods of the astronomical forcing, the isotopic response to this forcing will exhibit phase lags that are significant fractions of the forcing periods. At each period the lag will be different, depending on the period, on the nature of the physical system, and on the magnitude of the system's time constant. The problem is to estimate these phase lags. We do this by assuming that climate is a time invariant, single-exponential system, i.e., we assume that the rate of the response at any instant is proportional to the magnitude of the forcing. The impact such a (linear) system has on phase ( $\phi$ ) is well known. For steady state, it is given by  $\phi = -\arctan 2\pi f T$ , where  $T$  is the time constant and  $f$  the forcing frequency (16,35). The problem of estimating phase lags therefore reduces to that of estimating  $T$ . Here we follow the work of Imbrie and Imbrie (14), who based their estimate of  $T$  on data spanning an interval of time over which radiometric control is reasonably good (the past 127 KY). This estimate of  $T$  is  $17 \text{ KY} \pm 3 \text{ KY}$ . As shown in Table 3, an error of 3 KY in our estimate of  $T$  introduces discrepancies in our estimates of time lags that are on the order of 400 years.

The assumption stated above could be employed in various ways to develop a tuning strategy. We choose to pass the obliquity and precession signals through a single-exponential system with a time constant of 17 KY, and use the output curves as our tuning targets (see Fig. 9). The phase of each frequency component in these output curves is shifted by an amount that is fixed by the assumed time constant.

Data Processing. Each of these phase-shifted orbital curves can be regarded as a prediction of the isotopic signal over a narrow frequency band. We therefore apply phase-free digital filters to extract the appropriate frequency components from the raw isotopic data, and match this curve of filtered data against the corresponding phase-shifted orbital curve. Specifically, we attempt to match the phase of each excursion of a filtered curve with the phase of a corresponding excursion in an orbital curve. Except for portions of the record which lie near radiometric control points, a reasonably good phase lock can be achieved fairly easily -- provided that attention is confined to one orbital curve at a time. If, however, one attempts to achieve a satisfactory phase lock with the obliquity and precession curves simultaneously, the degrees of freedom available to the investigator (and the simplicity of the tuning task) is substantially decreased, even at stratigraphic levels that are far re-

Table 3 Predicted phases of  $\delta^{18}\text{O}$  responses at selected periods of orbital forcing, assuming a linear (exponential) system with time constants of 14 KY, 17 KY, and 20 KY.

Orbital Forcing	Period (KY)	Phase (°)			Time Lag (KY)		
		14 KY	17 KY	20 KY	14 KY	17 KY	20 KY
Obliquity	41	- 65	- 69	- 72	7.4	7.9	8.2
Precession	23	- 75	- 78	- 80	4.8	5.0	5.1
Precession	19	- 78	- 80	- 81	4.1	4.2	4.3

moved from radiometric time control.

In using this technique, the pass-band of a given filter must be wide enough to capture essentially all of the frequencies in the corresponding orbital curve. In the early phases of the tuning process, it must also be wide enough to capture isotopic frequencies which, although causally related to the orbital parameter under study, have been shifted across the spectrum by inaccuracies in the chronology. Yet the pass-bands must not be so wide as to encroach on concentrations of isotopic variance related to orbital influences other than the one being investigated. For studies of the precession band, the filter that we have designed to meet these constraints passes more than 50 per cent of the signal at periods between 17 KY and 27 KY; for the obliquity band, our filter passes the same fraction of the signal between 35 KY and 50 KY (see Table 4 and Fig. 10).

In using filters to tune the geologic record we make a basic assumption, namely, that the only significant concentrations of isotopic variance which occur within the pass-band of our filters represent responses to orbital forcing.

Control Points. Previous attempts to tune the isotopic record against orbital curves have limited the number of control points in the depth-vs.-age function to 17. In order to allow for changes in accumulation rate that occur at many places in our cores, we expand the number of control points as required. For reasons discussed above, most of the controls are placed at isotopic events studied and named by Prell et al. (27). Additional controls are added between these events wherever there is evidence of a change in accumulation rate.

Independent Evaluation. Criteria independent of the tuning process are used to evaluate the final time scale. One such criterion is the extent to which orbital and isotopic variations are coherent, i.e., the extent to which the amplitudes of excursions in one signal (and in a given frequency band) are proportional to the amplitudes of corresponding excursions in the other signal (and in the same frequency band). This property is conventionally measured by a coefficient of coherency, which is essentially a correlation coefficient calculated at zero phase and over a narrow frequency band (16). Following the lead of Kominz et al. (18) we will evaluate the time scale by inspecting a coherency spectrum, and pay particular attention to coherencies at three periods: 19 KY, 23 KY, and 41 KY. As shown on Figure 3, each of these narrow-band variations in orbital geometry has a distinctive time domain pattern.

Table 4 Weights of band-pass filters used in this paper. See (11) and (13) for description of numerical procedures.

22 KY Filter		41 KY Filter	
Lag ( $\pm$ KY)	Weight	Lag ( $\pm$ KY)	Weight
0	.080	0	.077
2	.066	5	.055
4	.030	10	.003
6	-.016	15	-.050
8	-.054	20	-.073
10	-.072	25	-.055
12	-.064	30	-.008
14	-.036	35	-.039
16	.002	40	.061
18	.034	45	.047
20	.051	50	.010
22	.049	55	-.027
24	.031	60	-.045
26	.006	65	-.036
28	-.016	70	-.010
30	-.027	75	.016
32	-.027	80	.028
34	-.019	85	.022
36	-.006	90	.007
38	.004	95	-.007
40	.010	100	-.014
42	.011	105	-.012
44	.008	110	-.004
46	.004	115	.003
48	-.001	120	.006
50	-.002	125	.006
-	-	130	.001

Another way of evaluating a time scale is to calculate depth-vs.-age functions for different cores. Given the prevalence of stratigraphic disturbances, abrupt shifts in this function are to be expected in any given core. However, the occurrence of abrupt shifts at the same time in cores from different sedimentary regimes would suggest that the shifts were artifacts of tuning.

#### Application of the Strategy

The application of this strategy to our cores can be summarized in terms of five sequential steps: (1) stratigraphic analysis; (2) development of an initial, radiometrically controlled time scale; (3) orbital tuning of individual cores; (4) inspec-

tion of depth-vs.-age plots; and (5) stacking.

Step 1 : Stratigraphic analysis. Inspection of the isotopic curves plotted as a function of depth in core (Fig. 4) reveals a number of inconsistencies that we interpret as evidence of stratigraphic disturbance. A conspicuous example occurs in Stage 5 (the isotopically light interval lying immediately above the 6.0 stage boundary). In three of our cores (V22-174, V30-40, and RC11-120), there are three conspicuous peaks, referred to in this paper as 5.1, 5.3, and 5.5. Because this pattern is consistent with dozens of high-resolution records previously analyzed, and inconsistent with the low-resolution records in cores V28-238 and DSDP502, we conclude that these two cores are disturbed in Stage 5. This conclusion is supported by independent evidence. In DSDP502, Prell et al. (26) report biostratigraphic evidence of a coring gap at this level; and in core V28-238 Prell et al. (27) report sedimentological evidence at this level of a disturbance associated with a coring gap. Another example of a stratigraphic inconsistency occurs in Stage 11 (the isotopically light interval near 700 cm in core V28-238). At depths from 723 cm to 753 cm in this core, there is a shelf of light values that has no counterpart in V22-174, in DSDP502, or in many other cores. A suspicion that the Stage 11 shelf in V28-238 is an artifact is strongly supported by sedimentological evidence of a disturbance at a core break (27). We conclude that this 30-cm section of core V28-238 represents a stretching of the record during core recovery, and have removed the corresponding data points from our files before tuning. Although we have not found it necessary to eliminate other raw data, the identification of stratigraphic inconsistencies played a crucial role in guiding our selection of control points.

Step 2 : Development of an initial time scale. Our initial time scale (Fig. 5) assumes that the accumulation rate was constant at each coring site between six stratigraphic levels. The first level is that of the core tops, where there is stratigraphic evidence of a near zero age. The remaining five control points are stratigraphic levels for which radiometric age estimates (Table 5) are available: two isotopic events in Stage 2 with radiocarbon ages of about 18 KY and 21 KY; the 6.0 isotopic stage boundary, taken as 127 KY; the Bruhnes-Matuyama magnetic reversal, taken as 730 KY; and the magnetic reversal at the top of the Jaramillo event, taken as 900 KY. Although the last-named event does not occur in any of the cores studied here, it nevertheless provides an important maximum age of the lowermost sample in V28-238. A biostratigraphic analysis of this core (37), indicates that the bottom of V28-238 is very close to the top of the Jaramillo interval. In our initial time scale we have therefore arbitrarily fixed the age of the bottom of this core as 890 KY.

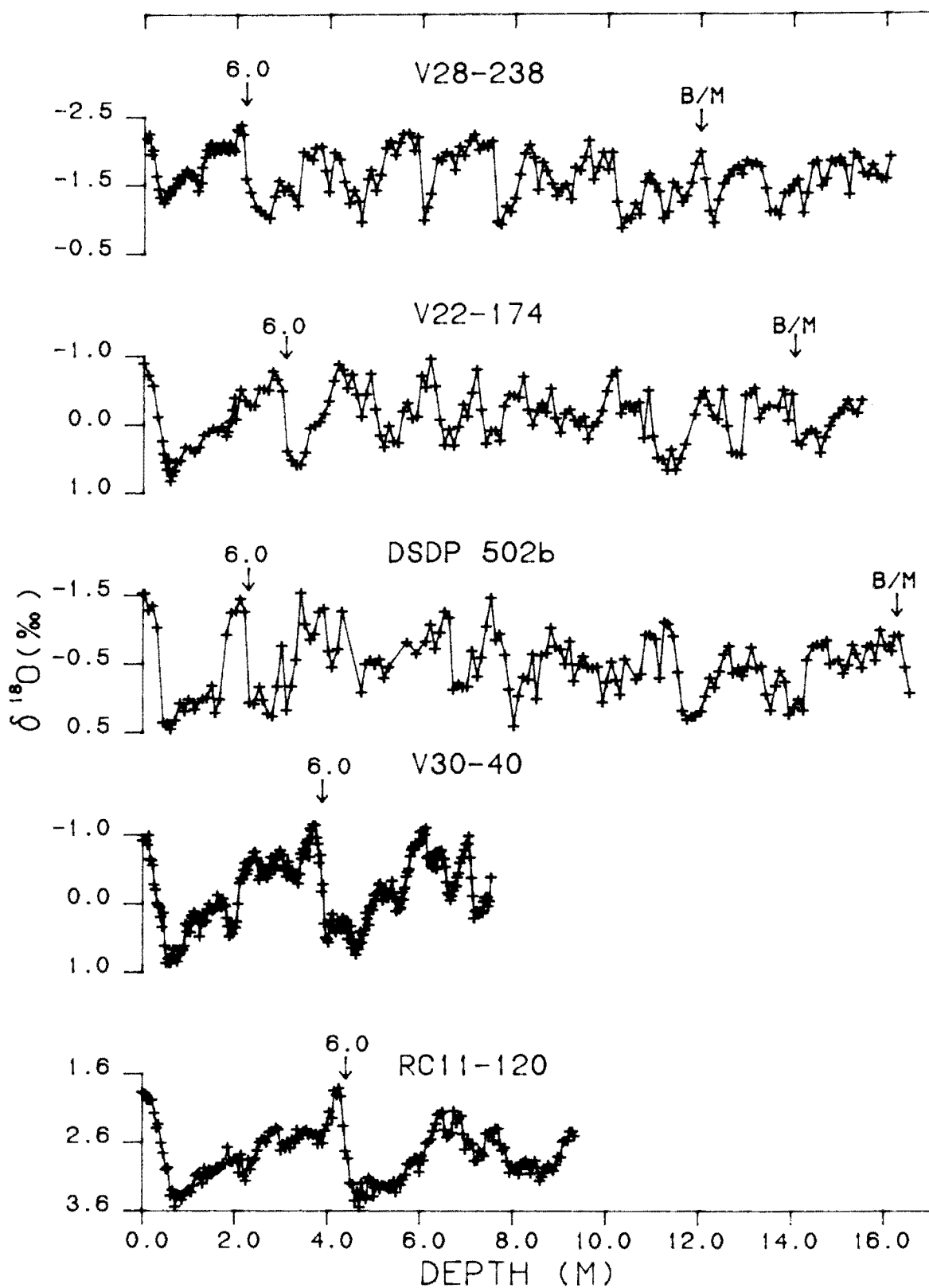


Figure 4 Variations in  $\delta^{18}\text{O}$  as a function of depth in five deep-sea cores. Two important stratigraphic levels are labeled as follows : 6.0 for the boundary between isotope stages 5 and 6; and B/M for the magnetic reversal at the Brunhes-Matuyama boundary. See Table 1.



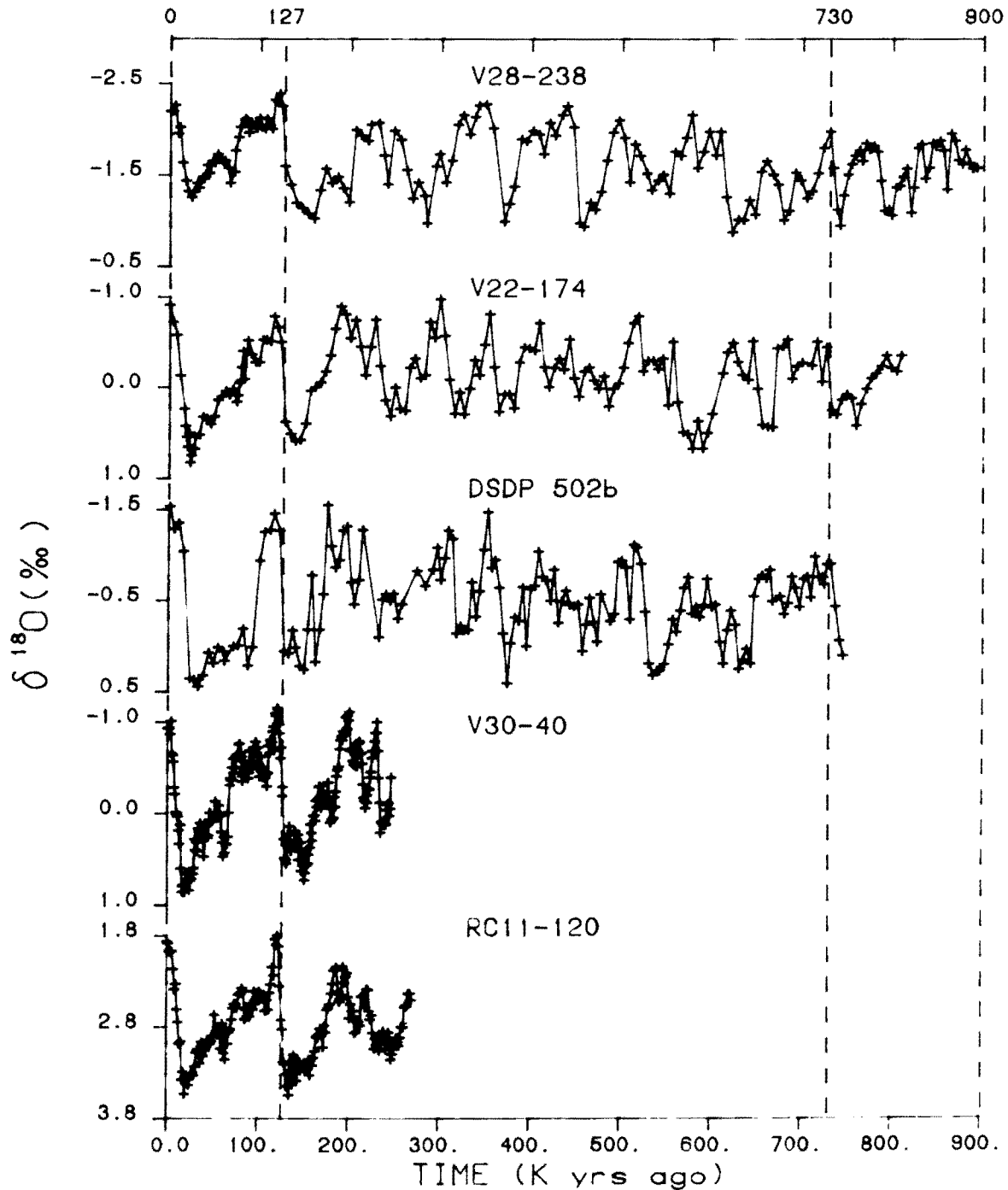


Figure 5 Variations in  $\delta^{18}\text{O}$  as a function of estimated time in five deep-sea cores. The time scale is derived by linear interpolation between (and extrapolation beyond) control points at 127 KY, 730 KY BP. For details, see text and Table 5.

Table 5 Radiometric ages for stratigraphic levels used as control points in this study.

Level	Age (KY)	Core	$\delta^{18}\text{O}$ Reference	Dating
Upper $\delta^{18}\text{O}$ Stage 2 (2.22)	17.8 $\pm$ 1.5	V19-188	(25, 43)	(25)
		CH22KW31	(24)	(24)
		V34-101	(43)	(43)
Lower $\delta^{18}\text{O}$ Stage 2 (2.24)	21.4 $\pm$ 2	V34-88	(43)	(43)
$\delta^{18}\text{O}$ Termination II (6.0)	127 $\pm$ 6	V12-122	(4)	(4, 31)
B/M Magnetic Boundary	730 $\pm$ 11	V28-238	(30, 32)	(20, 44)
		V22-174	(36)	(20, 44)
		DSDP502b	(26)	(20, 44)
Top Jaramillo Event	900 $\pm$ 14	V28-238	(30, 32)	(20, 44)

Step 3 : Orbital tuning. The tuning process is iterative, and begins with the initial time scale just described. At each iteration, digital filters centered at periods of 22 KY and 41 KY are applied to the data, and the phase of each excursion in the resulting curves is compared with the phase of excursions in the corresponding target curves. If significant phase differences occur between either pair of curves, an appropriate adjustment is made in the age of one or more control points, and the filtering process repeated. Midway in this process, the radiometric time constraints at the 6.0 and B/M boundaries are removed. The process is continued until the investigator is satisfied that an optimum phase lock has been achieved in both frequency bands. In our final time scale (Fig. 6 and Table 6), the number of non-radiometric control points used within the Brunhes ranges from 56 in V22-174 to 72 in DSDP502; the tuned ages of the 6.0 and B/M boundaries are 128 KY and 734 KY, respectively; and the age of the bottom sample in V28-238 is 892 KY.

This procedure can fairly be described as ungainly, in that the results presented here required approximately 120 iterations. But the application of this chronology to any new core is quite straightforward. Having identified as many of the isotopic events listed in Table 6 as possible, the investigator simply uses our estimate of the ages of these events and interpolates linearly between them.

Step 4 : Depths-vs.-age plots. The set of depth-vs.-age functions shown in Figure 7 provides some welcome support for the assumptions used in tuning. Each curve is fairly smooth over considerable intervals, and the sharp inflections that are present do not occur in all cores simultaneously.

Step 5 : Stacking. After adjusting the record in each core to have zero mean and unit standard deviation, the normalized curves (plotted on the new time scale) were superimposed, sampled at intervals of 1 KY, and averaged (Fig. 8). To avoid averaging data that are known to be atypical of records having greater resolution, short sections of Stage 5 in V28-238, DSDP502, and V22-174 were removed before stacking. This signal was then smoothed with a 9-point Gaussian filter (Table 7).

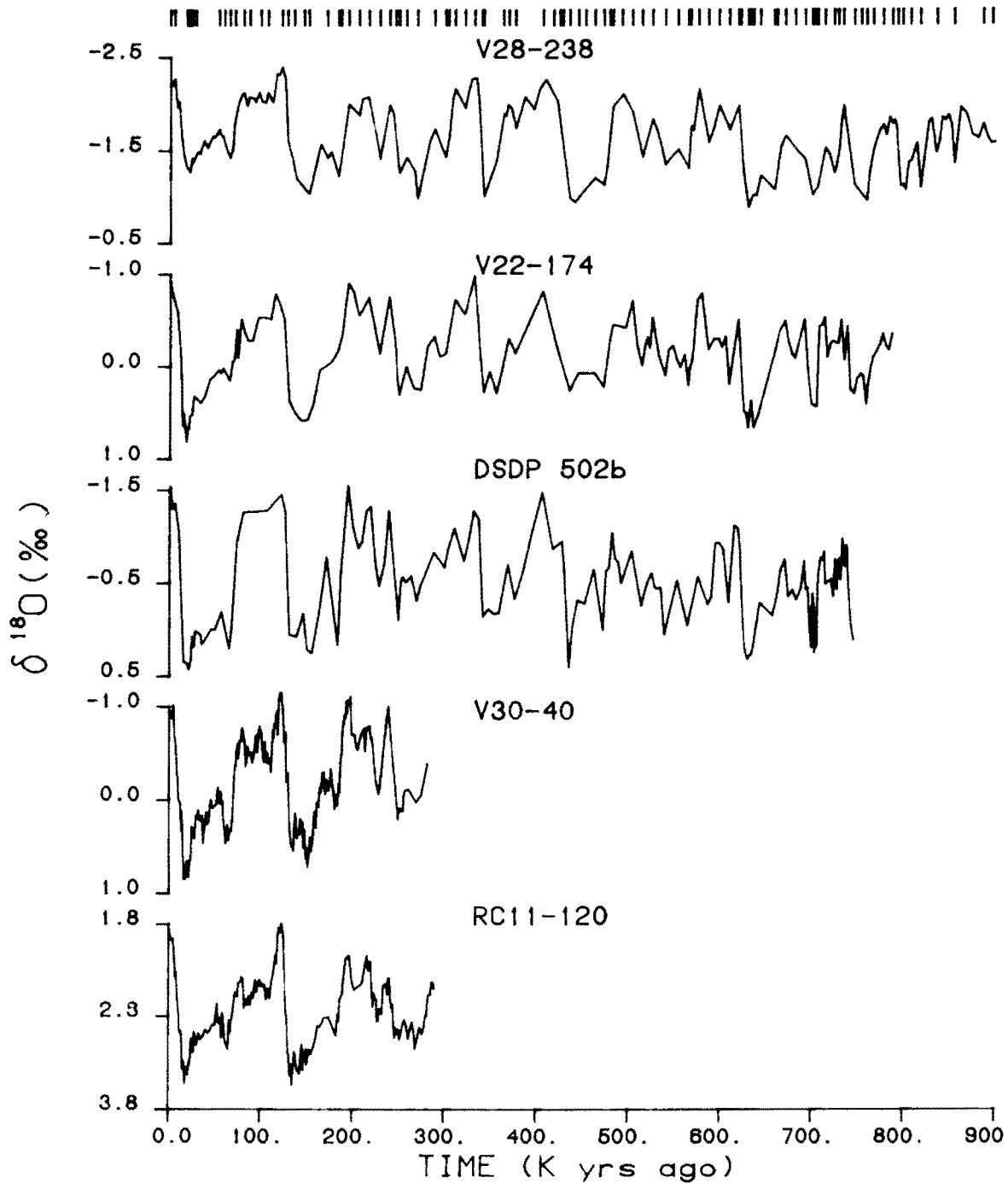


Figure 6 Variations in  $\delta^{18}O$  plotted on the SPECMAP time scale in five deep-sea cores. On this time scale, the 6.0 and B/M boundaries shown on Figs. 4 and 5 are dated at 128 KY and 734 KY, respectively. Small vertical lines at the top of the figure indicate time-scale control points (Table 6).

Table 6 Control points for the SPECMAP time scale. Isotopic events labeled 2.0, 3.0, etc., are stage boundaries as defined by Shackleton and Opdyke (32) in V28-238. Other numbered isotopic events are local maxima and minima of  $\delta^{18}\text{O}$  curves, as defined by Prell et al. (27). Unnumbered events are changes in sedimentation rate recognized in one core only. Zero age for core tops is an inference based on stratigraphic analysis. Ages marked (\*\*) are based on radiocarbon measurements (Table 5). The age marked (\*) relates to the isotopically heaviest excursion in the smoothed, stacked record for stage 2, as determined by interpolation between radiocarbon-dated levels. All other ages given without parentheses have been determined by orbital tuning methods. An age for a stage boundary given in parenthesis is determined by interpolation between adjacent ages with reference to the stratigraphic level of the corresponding event in V28-238. A depth given without parentheses represents an isotopic event recognized in a particular core and used there as time control. A depth in parentheses represents a stage boundary not used as time control in a particular core; this level has been determined by interpolation between adjacent levels with reference to the age of the corresponding event in column 2. Depths below 723 cm in V28-238 are 30 cm less than specified in (32) to allow for the effect of a core break.

Event	Age (KY)	Depth in Core (cm)				
		V30-40	RC11-120	V28-238	V22-174	DSDP502b
Top	0	0	0	0	0	0
1.1	6	12	-	10	-	-
2.0	12	33	45	22	26	33
2.22	17.8 <sup>**</sup>	58.5	70	-	-	47
2.2	19 <sup>*</sup>	-	-	42	57	-
2.24	21.4 <sup>**</sup>	75	85	-	-	59
3.0	24	91.5	110	55	80	74
3.1	28	-	135	-	100	99
3.3	53	162	185	91	150	-
4.0	59	183	215	111	175	154
4.2	65	195	225	115	180	157
5.0	71	208	250	128	192	178
5.1	80	241.5	290	145	-	191
5.2	87	261	-	-	235	-
-	94	-	335	-	-	-

Event	Age (KY)	Depth in Core (cm)				
		V30-40	RC11-120	V28-238	V22-174	DSDP502b
-	95	279	-	-	-	-
5.3	99	297	-	-	255	-
5.4	107	-	380	-	-	202
-	110	-	-	-	270	-
5.5	122	370.5	420	210	-	210
6.0	128	387	440	220	307	227
6.2	135	399	470	-	-	235
6.3	146	-	490	-	-	252
6.4	151	462	550	271	-	275
6.5	171	522	592	302	-	300
-	176	540	-	-	-	-
6.6	183	555	600	332	-	310
7.0	(186)	567	612	(335)	395	330
7.1	194	606	645	343	420	340
7.2	205	627	665	364	440	360
-	212	633	-	-	-	-
7.3	216	642	675	384	450	386
7.4	228	666	722	399	470	408
7.5	238	705	760	410	490	430
8.0	(245)	(713)	788	(430)	500	450
8.2	249	717	808	443	520	472
8.3	257	742	828	452	530	500
8.4	269	747	860	468	545	520
-	281	753	-	-	-	-
8.5	287	-	928	489	570	570
8.6	299	-	-	501	-	591
9.0	(303)	-	-	(510)	595	611
9.1	310	-	-	531	600	622
9.2	320	-	-	543	610	631
9.3	331	-	-	565	620	651
10.0	(339)	-	-	(595)	(644)	668
10.2	341	-	-	603	650	671
11.0	362	-	-	630	(681)	709
11.1	368	-	-	658	690	711
11.2	375	-	-	671	700	722
-	395	-	-	691	-	-
11.3	405	-	-	710	720	752
11.4	416	-	-	-	-	762
-	420	-	-	723	-	-

Event	Age (KY)	Depth in Core (cm)				
		V30-40	RC11-120	V28-238	V22-174	DSDP502b
12.0	(423)	-	-	(725)	(732)	(768)
12.1	426	-	-	-	-	771
12.2	434	-	-	733	740	801
-	439	-	-	741	-	-
12.31	443	-	-	-	750	822
12.32	451	-	-	-	-	831
12.33	461	-	-	752	760	842
12.4	471	-	-	761	770	851
13.0	(478)	-	-	(781)	780	(871)
13.11	481	-	-	792	790	882
13.12	491	-	-	-	-	912
13.13	502	-	-	812	820	922
13.2	513	-	-	821	840	931
14.0	524	-	-	830	880	951
14.2	538	-	-	860	900	993
14.3	552	-	-	880	-	1011
14.4	563	-	-	891	960	1031
15.0	(565)	-	-	(900)	(972)	1037
15.1	574	-	-	930	1015	1040
15.2	585	-	-	940	1030	1066
15.3	596	-	-	960	1050	1095
15.4	607	-	-	971	1080	1116
15.5	617	-	-	980	1090	1133
16.0	(620)	-	-	(985)	1095	1150
16.22	628	-	-	1000	1130	1176
16.23	631	-	-	-	-	-
16.24	634	-	-	-	1150	1206
16.3	641	-	-	1030	-	1226
16.4	656	-	-	1040	-	1236
17.0	(659)	-	-	(1045)	(1194)	(1243)
17.1	668	-	-	1060	1210	1266
17.2	679	-	-	-	1240	-
17.3	689	-	-	1080	1250	1313
18.0	689	-	-	1080	1250	1313
18.22	697	-	-	1090	-	1356
18.23	700	-	-	-	1280	-
18.24	703	-	-	1100	-	1426
18.3	711	-	-	1111	1320	1475

Event	Age (KY)	Depth in Core (cm)				
		V30-40	RC11-120	V28-238	V22-174	DSDP502b
18.4	721	-	-	1131	-	1512
19.0	(726)	-	-	(1150)	1372	1561
19.1	731	-	-	1171	-	1592
20.0	(736)	-	-	(1180)	1403	1640
20.22	743	-	-	1191	1420	1664
20.23	750	-	-	-	1440	-
20.24	756	-	-	1200	1460	-
21.0	(763)	-	-	(1220)	1490	-
21.1	774	-	-	1251	1520	-
21.3	784	-	-	1280	1550	-
22.0	(790)	-	-	(1310)	-	-
22.2	795	-	-	1331	-	-
22.3	804	-	-	-	-	-
22.4	814	-	-	1391	-	-
-	832	-	-	1433	-	-
-	851	-	-	1490	-	-
-	882	-	-	1540	-	-
-	892	-	-	1565	-	-

Table 7 The stacked, smoothed oxygen-isotope record as a function of age in the SPECMAP time scale. Ages in KY BP are given at steps of 2 KY. Isotopic variations expressed in standard deviation units around a zero mean.

0	-2.09	210	-1.12	420	-0.68	630	1.84
2	-1.91	212	-1.23	422	-0.53	632	1.77
4	-1.74	214	-1.35	424	-0.34	634	1.79
6	-1.41	216	-1.40	426	-0.10	636	1.69
8	-1.02	218	-1.27	428	0.25	638	1.49
10	-0.44	220	-0.01	430	0.69	640	1.25
12	0.29	222	-0.64	432	1.17	642	1.10
14	1.01	224	-0.31	434	1.50	644	1.05
16	1.58	226	-0.03	436	1.49	646	1.01
18	1.81	228	0.12	438	1.34	648	0.98



20	1.78	230	-0.02	440	1.19	650	0.94
22	1.65	232	-0.31	442	1.06	652	0.90
24	1.38	234	-0.68	444	0.97	654	0.86
26	1.14	236	-1.02	446	0.95	656	0.74
28	1.02	238	-1.18	448	0.93	658	0.51
30	0.96	240	-1.03	450	0.91	660	0.23
32	0.94	242	-0.65	452	0.87	662	-0.05
34	0.94	244	-0.20	454	0.79	664	-0.25
36	0.96	246	0.30	456	0.71	666	-0.38
38	0.94	248	0.70	458	0.64	668	-0.40
40	0.85	250	0.78	460	0.58	670	-0.23
42	0.77	252	0.66	462	0.61	672	-0.02
44	0.67	254	0.52	464	0.73	674	0.11
47	0.59	256	0.40	466	0.87	676	0.18
48	0.56	258	0.37	468	1.01	678	0.24
50	0.50	260	0.43	470	1.08	680	0.26
52	0.38	262	0.50	472	0.88	682	0.21
54	0.37	264	0.55	474	0.44	684	0.11
56	0.41	266	0.67	476	0.03	686	-0.01
58	0.50	268	0.85	478	-0.35	688	-0.12
60	0.68	270	0.89	480	-0.70	690	0.05
62	0.89	272	0.77	482	-0.86	692	0.46
64	1.00	274	0.60	484	-0.82	694	0.93
66	0.93	276	0.42	486	-0.79	696	1.33
68	0.66	278	0.21	488	-0.76	698	1.40
70	0.22	280	-0.01	490	-0.71	700	1.42
72	-0.24	282	-0.19	492	-0.68	702	1.36
74	-0.53	284	-0.35	494	-0.69	704	0.76
76	-0.69	286	-0.47	496	-0.74	706	0.08
78	-0.88	288	-0.46	498	-0.82	708	-0.21
80	-0.98	290	-0.31	500	-0.91	710	-0.32
82	-0.77	292	-0.15	502	-0.89	712	-0.16
84	-0.48	294	-0.05	504	-0.68	714	0.10
86	-0.45	296	0.02	506	-0.36	716	0.15
88	-0.47	298	0.05	508	-0.07	718	0.18
90	-0.46	300	-0.05	510	0.18	720	0.26
92	-0.52	302	-0.30	512	0.37	722	0.21
94	-0.71	304	-0.61	514	0.35	724	0.08
96	-0.80	306	-0.93	516	0.15	726	-0.14
98	-0.91	308	-1.20	518	-0.04	728	-0.43
100	-0.96	310	-1.34	520	-0.15	730	-0.55
102	-0.80	312	-1.31	522	-0.31	732	-0.49
104	-0.69	314	-1.19	524	-0.45	734	-0.42
106	-0.59	316	-1.06	526	-0.37	736	-0.18
108	-0.51	318	-0.95	528	-0.17	738	0.39
110	-0.50	320	-0.91	530	0.02	740	0.91
112	-0.73	322	-1.03	532	0.17	742	1.19
114	-1.19	324	-1.23	534	0.34	744	1.25
116	-1.53	326	-1.45	536	0.60	746	1.18
118	-1.72	328	-1.65	538	0.79	748	1.14

120	-1.98	330	-1.79	540	0.72	750	1.15
122	-2.12	332	-1.72	542	0.54	752	1.22
124	-1.89	334	-1.40	544	0.40	754	1.40
126	-1.19	336	-0.84	546	0.30	756	1.48
128	-0.26	338	-0.04	548	0.26	758	1.18
130	0.51	340	0.75	550	0.24	760	0.75
132	1.05	342	1.12	552	0.26	762	0.40
134	1.33	344	1.07	554	0.34	764	0.18
136	1.35	346	0.94	556	0.42	766	0.03
138	1.28	348	0.86	558	0.49	768	-0.10
140	1.32	350	0.86	560	0.64	770	-0.23
142	1.33	352	0.88	562	0.80	772	-0.36
144	1.26	354	0.86	564	0.65	774	-0.40
146	1.26	356	0.74	566	0.33	776	-0.30
148	1.41	358	0.53	568	0.08	778	-0.24
150	1.57	360	0.28	570	-0.27	780	-0.31
152	1.58	362	0.03	572	-0.68	782	-0.42
154	1.45	364	-0.18	574	-0.94		
156	1.30	366	-0.38	576	-0.93		
158	1.07	368	-0.50	578	-0.77		
160	0.85	370	-0.43	580	-0.51		
162	0.60	372	-0.25	582	-0.22		
164	0.40	374	-0.07	584	0.03		
166	0.25	376	-0.03	586	0.11		
168	0.15	378	-0.15	588	-0.01		
170	0.11	380	-0.30	590	-0.25		
172	0.12	382	-0.46	592	-0.51		
174	0.18	384	-0.61	594	-0.67		
176	0.27	386	-0.73	596	-0.71		
178	0.47	388	-0.82	598	-0.65		
180	0.71	390	-0.90	600	-0.57		
182	0.83	392	-0.98	602	-0.48		
184	0.62	394	-1.07	604	-0.23		
186	0.11	396	-1.19	606	0.11		
188	-0.42	398	-1.35	608	0.15		
190	-0.88	400	-1.51	610	-0.15		
192	-1.31	402	-1.66	612	-0.51		
194	-1.62	404	-1.77	614	-0.79		
196	-1.62	406	-1.77	616	-0.90		
198	-1.41	408	-1.64	618	-0.62		
200	-1.17	410	-1.46	620	0.09		
202	-0.99	412	-1.27	622	0.86		
204	-0.88	414	-1.08	624	1.42		
206	-0.88	416	-0.91	626	1.77		
208	-1.00	418	-0.79	628	1.92		

---

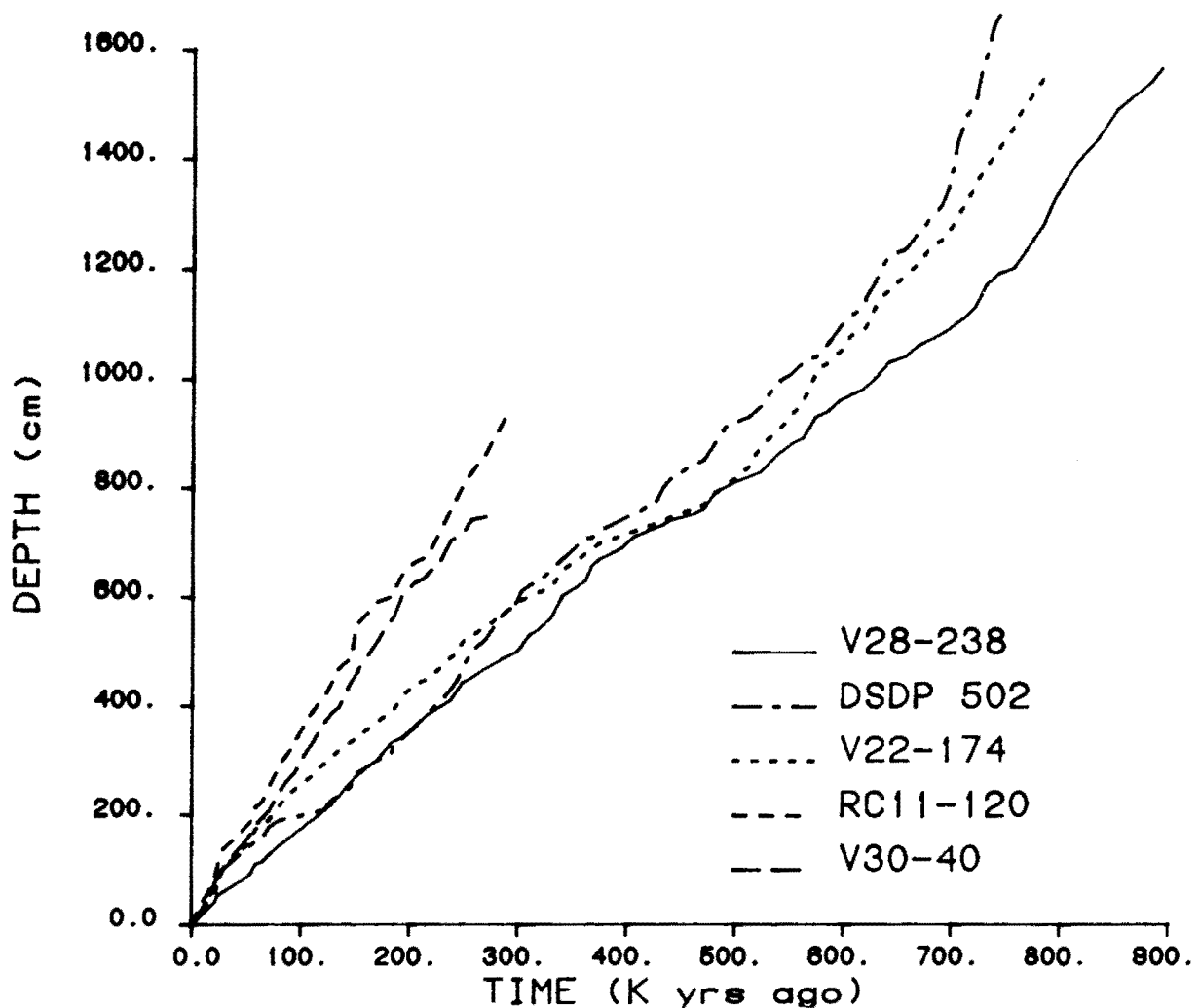


Figure 7 Depth vs. age in the SPECMAP time scale for five deep-sea cores analyzed in this paper.

## DISCUSSION

### The SPECMAP Time Scale

Filtered data. In each of the cores studied here, a time scale was developed by using digital filters to lock the phase of isotopic and orbital signals over two frequency bands. The stacked isotope record provides a convenient way of inspecting the result (41). As shown by the filtered data on Figure 9, a reasonably good phase lock has been achieved. Ninety per cent of the local maxima and minima of the obliquity curve lie within  $\pm 3$  KY of corresponding points on the filtered isotopic curve. A similar analysis of curves related to precession shows that the discrepancies do not exceed  $\pm 2$  KY. In both frequency bands, moreover, the discrepancies are considerably smaller away from the extremes of the excursions -- a point that will be emphasized below in our analysis of the phase spectrum.

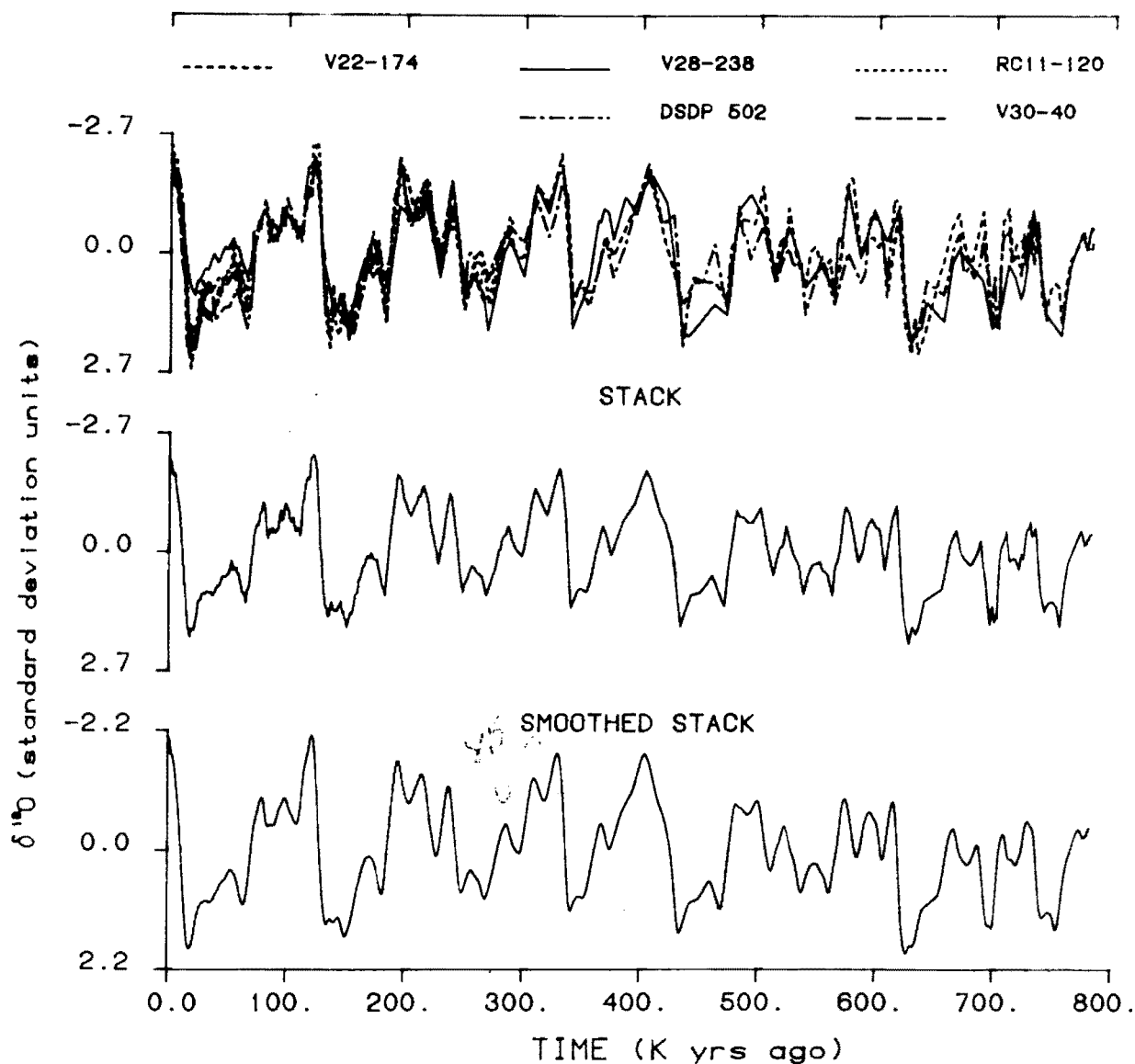


Figure 8  $\delta^{18}\text{O}$  variations in five deep-sea cores normalized and plotted on the SPECMAP time scale. In the top panel, data from each core has been normalized to zero mean and unit standard deviation. After interpolation at intervals of 1 KY, these curves have been averaged (middle panel), and smoothed with a 9-point Gaussian filter (bottom panel).

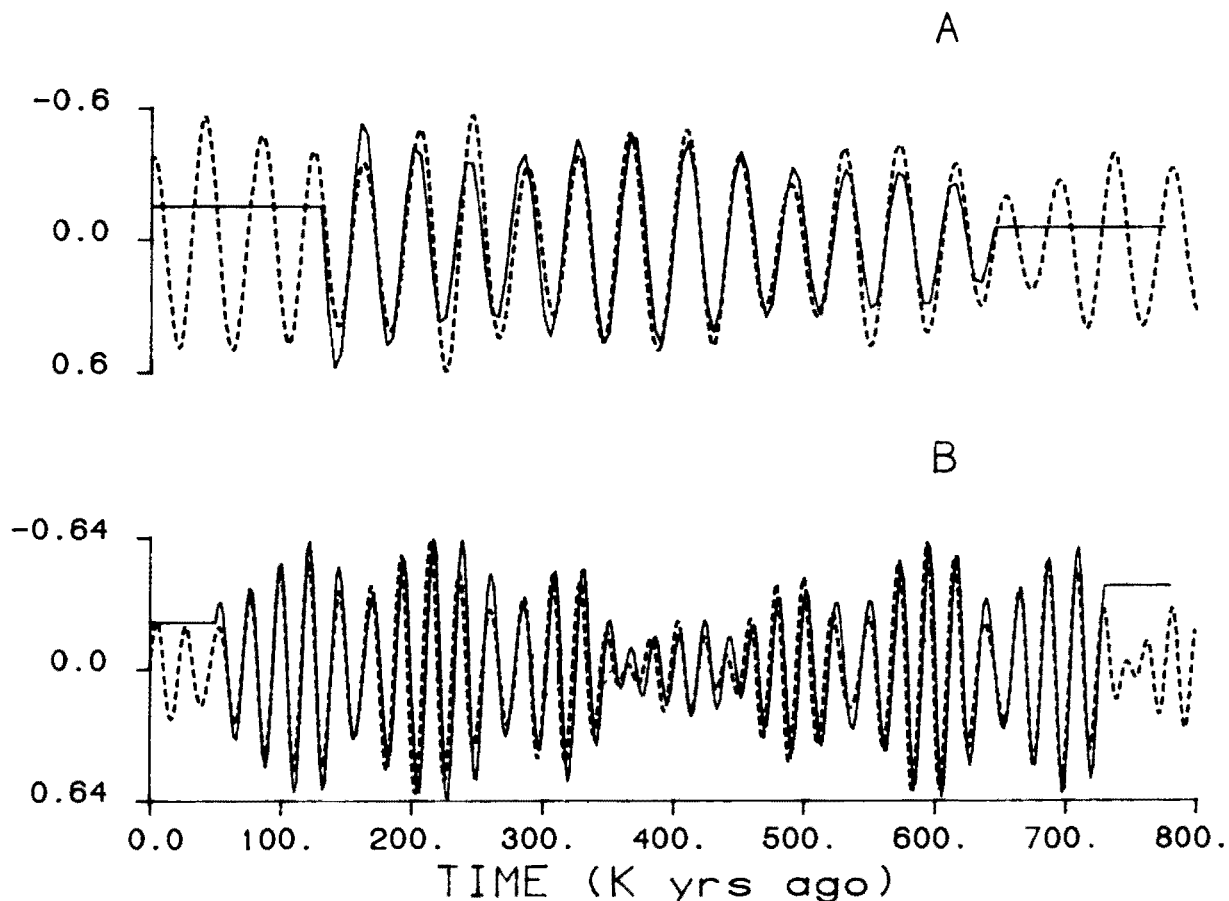


Figure 9 Variations in obliquity, precession, and the corresponding frequency components of  $\delta^{18}\text{O}$  over the past 800 KY. Dashed lines are phase-shifted versions of obliquity (A) and precession (B) curves. Solid lines are filtered versions of the stacked  $\delta^{18}\text{O}$  record plotted on the SPECMAP time scale. The filters used were centered on periods of 41 KY (A) and 22 KY (B). All curves have been transformed to have zero means with arbitrary scales.

An inspection of the filtered data on Figure 9 shows that the orbital and isotopic signals are strikingly coherent in both frequency bands. In other words, the magnitude of individual excursions in one curve tend to be proportional to corresponding excursions in the other.

Coherency spectrum. The techniques of cross-spectral analysis provide another way of analyzing the relationships between two signals. These techniques are more powerful than filtering because they make it possible to examine coherency (and phase) across the entire range of statistically visible frequencies, and to do so at a higher resolution than is practical with filters. We have performed such an analysis on two signals: (1) the raw, stacked isotopic data, plotted on the SPECMAP time scale; and (2) a signal constructed by normalizing and stacking

curves of eccentricity, obliquity, and precession (Fig. 2). None of the individual components that make up this signal (which we will refer to as ETP) has been shifted in phase. However, we have reversed the sign of the precession index so that positive excursions in this core have the same climatic direction in the Northern Hemisphere as positive excursions in eccentricity and obliquity. Our object in performing cross-spectral analysis against the ETP curve, rather than against the individual orbital curves, is purely one of convenience, namely, to obtain a compact summary of orbital-isotopic relationships across the entire visible spectrum in a single diagram. Within each frequency band of interest, the results using ETP could be duplicated exactly by calculating a cross spectrum against the appropriate individual orbital curve.

In examining the coherency spectrum (Fig. 10), we first discuss the periods of variation in precession and obliquity (19 KY, 23 KY, and 41 KY), for it is over this part of the spectrum that the tuning was done. The measured coherencies (0.94, 0.97, and 0.93, respectively) are not only surprisingly high in absolute value, but lie well above the 5 per cent significance level (0.78). These peaks in the coherency spectrum coincide exactly with peaks in the isotopic and orbital spectra. Turning now to the low-frequency end of the spectrum, we find coherencies as high as 0.92 in the frequency band associated with the 100 KY eccentricity cycle. This peak in the coherency spectrum coincides approximately with conspicuous peaks in the isotopic and orbital spectra. Since the discovery of the 100-KY cycle (4,19), many investigators have been tempted to conclude that it is causally related in some way to variations in eccentricity (13,14,17). Our observation that variations in climate and eccentricity are strongly coherent in the 100-KY band is, we believe, the first compelling evidence in support of this idea.

These results -- and the fact that the tuned ages of 128 KY and 734 KY for the 6.0 and B/M boundaries agree with radiometric dates -- argue that the SPECMAP time scale is tightly constrained. To emphasize this point, we call attention to the diversity of the patterns of orbital variations in the 19 KY, 23 KY, 41 KY, and 100 KY frequency bands (Fig. 3). It is difficult to see how coherencies ranging from 0.92 to 0.97 could be achieved in all four frequency bands simultaneously as an artifact of the tuning procedure. We therefore conclude that the time scale presented in this paper is considerably more accurate than those developed earlier (13,17,18,22).

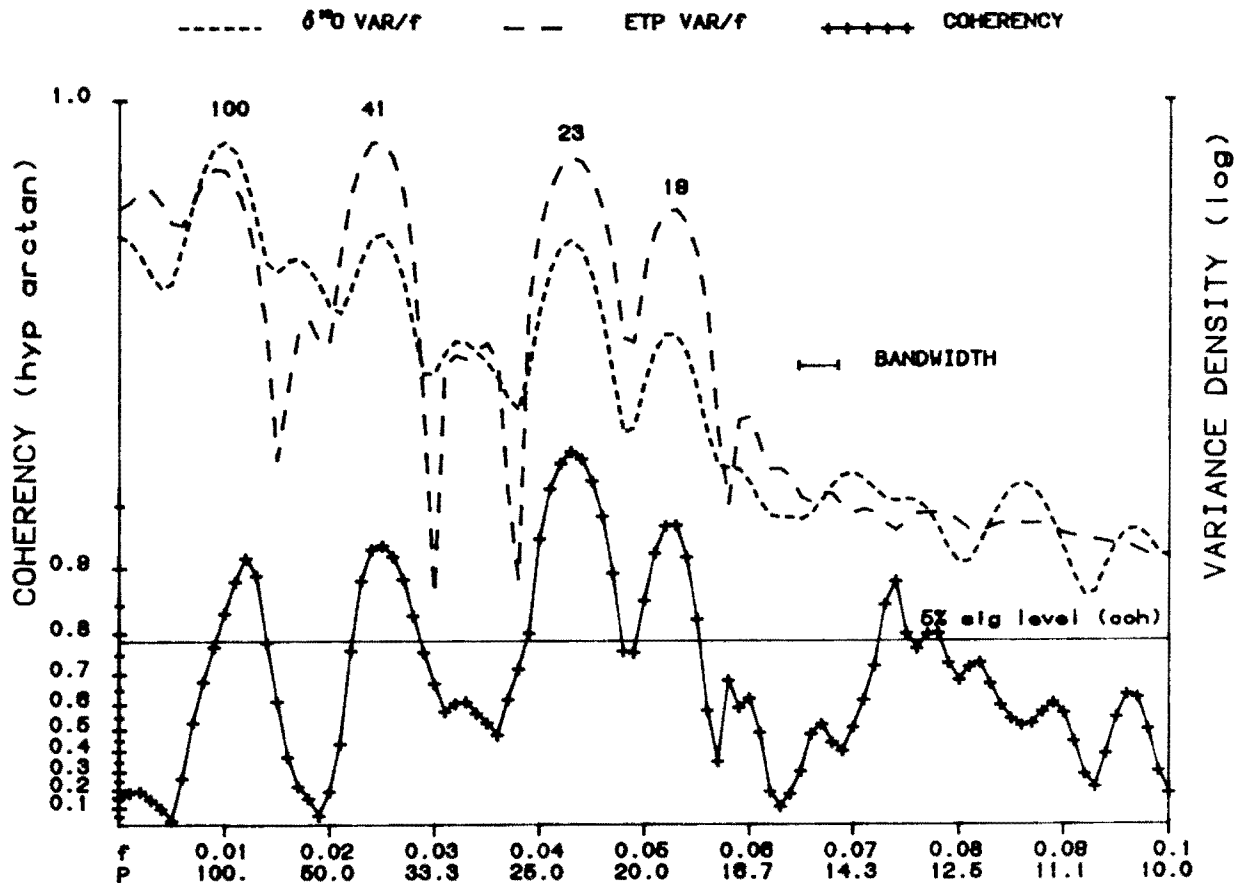


Figure 10 Coherency and variance spectra calculated from records of climatic and orbital variation spanning the past 780 000 years. Two signals have been processed: (1) ETP, a signal formed by normalizing and adding variations in eccentricity, obliquity, and precession; and (2)  $\delta^{18}\text{O}$ , the unsmoothed, stacked isotope record plotted on the SPECMAP time scale (Fig. 9). Top: variance spectra for the two signals are plotted on arbitrary log scales. Bottom: coherency spectrum plotted on a hyperbolic arctangent scale and provided with a 5% significance level. Frequencies are in cycles per thousand years.

Phase spectrum. The fundamental assumption used to develop our time scale is that isotopic phase lags at the frequencies of obliquity and precession are those of a single-exponential system with a time constant of 17 KY (Table 3). The extent that we have been able to adjust our time scale to fit this assumption has already been discussed in the context of plots showing filtered data and phase-shifted orbital curves (Fig. 9). Plots of this kind were crucial to the development of the SPECMAP time scale because they made it possible to examine phase relationships one cycle at a time. Having completed this iterative process, however, we can now extract additional information about

phase by calculating a phase spectrum. Diagrams of this kind have a number of useful properties: they integrate phase information over the entire length of the geologic record; they provide statistical summaries of the information (means and standard deviations) over a wide range of frequencies; and they achieve a higher resolution in the frequency domain than is practical with digital filters.

Two phase spectra are shown in Figure 11. One of these is a theoretical phase spectrum calculated on the assumption that the steady-state response to orbital forcing can be modeled as a single-exponential system with a time constant of 17 KY. The other curve, given with 95 per cent confidence intervals, shows the observed phase spectrum between the ETP signal and the stacked isotopic data plotted on the SPECMAP time scale. Considering the assumptions we used in tuning, it is hardly surprising that the observed phases lie close to the predicted phases in narrow bands centered on the main frequencies of obliquity and precession. We are, however, somewhat surprised that the observed and predicted phases match so well over the entire range of periods from 16 KY to 45 KY; and that the 95 per cent confidence intervals over this range are as small as they are. Expressed in terms of time shifts, the 95 per cent confidence intervals in the obliquity and precession bands are  $\pm 1.8$  KY and  $\pm 0.6$  KY, respectively.

At periods longer than about 50 KY, the observed phase spectrum in Figure 11 departs significantly from the predicted spectrum. One way of explaining this behavior is to postulate the existence of a resonance phenomenon acting near a period of 100 KY. This idea will be explored further in a later paper.

Accuracy. The phase spectrum of the stacked isotope record (Fig. 11) can be used as a basis for estimating the accuracy of the SPECMAP time scale. We start by assuming that the confidence intervals for the phase lags at the obliquity and precession frequencies (1.8 KY and 0.6 KY) reflect two types of uncertainty. Type 1 includes various kinds of observational error. Type 2 includes errors in our assumption that the climate system can be modeled over some 800 000 years as a time-invariant linear system. To these must be added our previous estimate of the error (0.4 KY) attached to the assumption of a 17 KY time constant (Type 3 error). In addition, errors in stratigraphic correlation caused by delay in ocean mixing (Type 4) must be considered. Here we use recent evidence that the mixing time of oceanic deep waters is about 500 years (34) to estimate the stratigraphic error as 0.25 KY. Assuming that these four types of error are independent and normally distributed, we combine them and estimate that the 95% confidence interval for control points in the SPECMAP time scale is  $\pm 2$  KY. However, our ability



to identify any given isotopic event in any given core is limited to one half of the sampling interval used in the relevant part of that core (Type 5 error). In the records studied here, this uncertainty ranges from 0.5 KY to 2.5 KY (Table 1). Our final estimate of the error in our chronology for any given core therefore ranges from 3 KY to 5 KY, depending on the sampling interval.

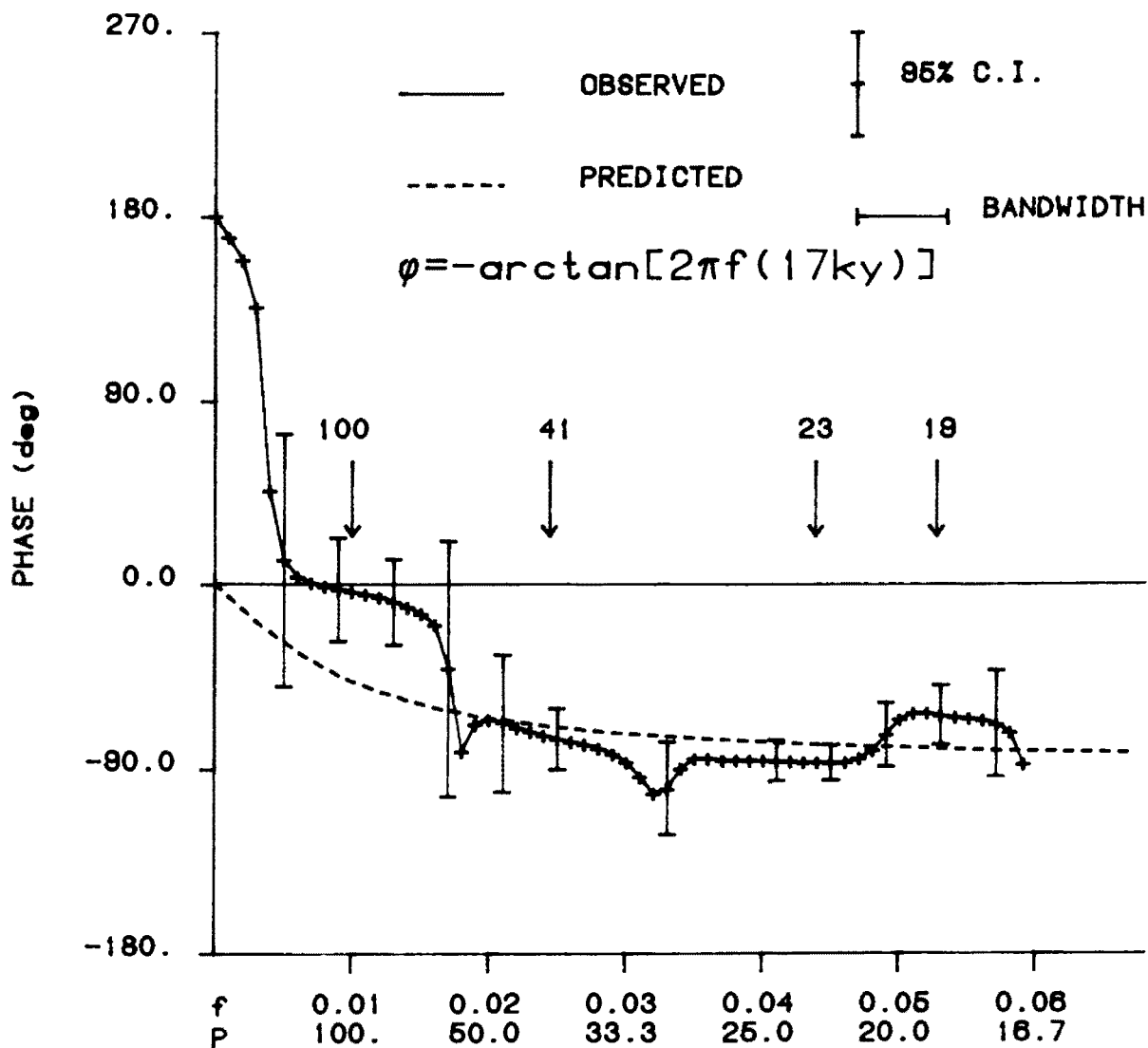


Figure 11 Theoretical and observed phase spectra relating climatic and orbital variation over the past 780 000 years. Negative phase indicates that climatic variation lags orbital variation. Dashed line: predicted phases (degrees) based on the response of a single-exponential system with a time constant of 17 KY. Solid line: observed phases calculated from orbital and  $\delta^{18}\text{O}$  signals described in Figure 10. Frequencies in cycles per thousand years.

The B/M magnetic reversal is a non-isotopic event recorded at particular stratigraphic levels in three of our cores (45). Ages for these levels, calculated by interpolation in the SPEC-MAP time scale, lie in the interval  $734 \text{ KY} \pm 3 \text{ KY}$ . It seems likely that the differences in these estimates reflect the operation of Type 1, Type 4, and Type 5 errors. Allowing for the effects of errors of Type 2 and Type 3, we estimate that the age of the B/M boundary is  $734 \pm 5 \text{ KY}$ . On this basis, Johnson's 790-KY estimate (17) is 50 000 years too old.

### The Astronomical Theory

Having developed a time scale that we believe is accurate to within 5 KY, we are now in a position to evaluate the astronomical theory empirically. Our main contribution to this goal is the coherency spectrum (Fig. 10). As discussed above, coherencies at the four main periods of astronomical forcing -- including the 100 KY eccentricity period -- are 0.92 or above. Since the square of any given coherency represents that fraction of the total observed variance that can be explained as a linear response to orbital forcing, we believe that as much as 85 per cent of the isotopic variance in each of four narrow frequency bands (centered on periods of 19 KY, 23 KY, 41 KY, and 100 KY) is forced in some way by orbital variation. By integrating the square of the coherency spectrum over the entire range of periods from 19 KY to 100 KY -- including frequencies at which no orbital variation occurs -- we estimate that some 60 per cent of the total isotopic variance observed over this part of the climatic spectrum is a response to orbital forcing. On average, therefore, Milankovitch mechanisms would explain at least 77 per cent of the amplitude of  $\delta^{18}\text{O}$  excursions observed in the records under study here. It seems highly likely that a satisfactory account of the residual variance that is not explained by orbital theory will require the consideration of internal stochastic mechanisms (12,18) as well as a search for external causes that are unrelated to celestial mechanics. But a careful study of the marine isotopic record leaves little room for doubt that variations in the geometry of the Earth's orbit are the main cause of the succession of late Pleistocene ice ages.

### CONCLUSIONS

1. Oscillations in five  $\delta^{18}\text{O}$  records obtained from pelagic foraminifera at open-ocean sites in low- and mid-latitudes are strongly correlated over the past 780 000 years. We infer that changes in the global volume of glacial ice are the dominant influence on this pattern.

2. A geologic time scale can be developed from a simple model in which the isotopic record is considered as the response of a single-exponential system being forced by variations in obliquity and precession. With a time constant of 17 KY, this model satisfactorily accounts for the amplitudes and phases of the isotopic signal over a range of periods from 16 KY to 50 KY.

3. In this new time scale, the age of the isotopic Stage 5 - Stage 6 boundary is  $128 \text{ KY} \pm 3 \text{ KY}$ , and the age of the Brunhes-Matuyama magnetic boundary is  $734 \text{ KY} \pm 5 \text{ KY}$ . Unlike some previously published time scales, the chronology presented here is consistent with radiometric dates for these boundaries ( $127 \text{ KY} \pm 6 \text{ KY}$  and  $730 \text{ KY} \pm 11 \text{ KY}$ , respectively).

4. At each of the main orbital periods that are resolvable in a record of this length (19 KY, 23 KY, 41 KY, and 100 KY), coherencies between orbital and isotopic signals exceed 0.9 and are highly significant statistically. In narrow frequency bands centered on these four frequencies, therefore, at least 85 per cent of the observed isotopic variance is linearly related to orbital forcing.

5. This empirical study of the marine isotopic record leaves little room for doubt that variations in the geometry of the Earth's orbit are the main cause of the succession of late Pleistocene ice ages.

#### ACKNOWLEDGEMENTS

We wish to acknowledge our debt to several people whose efforts made it possible for us to complete this paper in its present form. André Berger provided us with the digital results of his orbital computations. Angeline Duffy carried out over half of the complex, iterative calculations required to develop our time scale. Gordon Start helped with the tuning process, particularly in DSDP502. Rosalind Mellor accurately processed the words in our text and the numbers in our tables. We also acknowledge the support of a National Science Foundation grant NSF ATM80-18897 (SPECMAP) through the Climate Dynamics Section, Division of Atmospheric Sciences, the Seabed Assessment Program, International Decade of Ocean Exploration, Division of Ocean Sciences; and the Division of Polar Programs. We are also indebted to the National Science Foundation for its support of the Lamont-Doherty Geological Observatory core laboratory.

## REFERENCES

1. Berger, A.L. : 1976, *Astron. Astrophys.* 51, pp. 127-135;  
1977, *Celest. Mech.* 15, pp. 53-74.
2. Berger, A.L. : 1978, *Quaternary Research* 9, pp. 139-167.
3. Berger, A.L. : 1977, *Nature (Lond.)* 269, pp. 44-45.
4. Broecker, W.S., and Van Donk, J. : 1970, *Rev. Geophys. Space Phys.* 8, pp. 169-197.
5. Croll, J. : 1864, *Phil. Mag.* 28, pp. 121-137; 1875, "Climate and Time", Appleton, New York.
6. Dodge, R.E., Fairbanks, R.G., Benninger, L.W., and Maurrasse, F. : 1983, *Science* 219, pp. 1423-1425.
7. Duplessy, J.C., Delibrias, G., Turon, J.L., Pujol, C., and Duprat, J. : 1981, *Palaeogeog., -clim., -eol.* 35, pp. 121-144.
8. Emiliani, C. : 1955, *J. Geol.* 63, pp. 538-578.
9. Emiliani, C. : 1966, *Science* 154, pp. 851-857.
10. Fairbanks, R.G., and Matthews, R.K. : 1978, *Quaternary Research* 10, pp. 181-196.
11. Goodman, J. : 1960, *J. Franklin Inst.* 270, pp. 437-450.
12. Hasselmann, K. : 1976, *Tellus* 28, pp. 473-485.
13. Hays, J.D., Imbrie, J., Shackleton, N.J. : 1976, *Science* 194, pp. 1121-1132.
14. Imbrie, J., and Imbrie, J.Z. : 1980, *Science* 207, pp. 943-953.
15. Imbrie, J. : 1982, *Icarus* 50, pp. 408-422.  
Imbrie, J., and Imbrie, K.P. : 1979, "Ice Ages : Solving the Mystery", Enslow, Short Hills, N.J.
16. Jenkins, G.M., and Watts, D.G. : 1968, "Spectral analysis and its applications", Holden-Day, San Francisco.
17. Johnson, R.G. : 1982, *Quaternary Research* 17, pp. 135-147.
18. Kominz, M.A., Heath, G.R., Ku, T.-L., and Pisias, N.G. : 1979, *Earth Planet. Sci. Lett.* 45, pp. 394-410. Kominz, M.A., and Pisias, N.G. : 1979, *Science* 204, pp. 171-173.
19. Kukla, G. : 1968, *Current Anthropology* 9, pp. 37-39.  
Kukla, G.J. : 1970, *Geol. Foren. Stockholm Forh.* 92, pp. 148-180.
20. Mankinen, E.A., and Dalrymple, G.B. : 1979, *J. Geophys. Res.* 84, pp. 615-626.
21. Milankovitch, M. : 1920, "Théorie mathématique des phénomènes thermiques produits par la radiation solaire", Gauthiers-Villars, Paris; 1941, *Royal Serb. Acad., Spec. Publ.*, 133, pp. 1-633.
22. Morley, J.J., and Hays, J.D. : 1981, *Earth Planet. Sci. Lett.* 53, pp. 279-295.
23. Olausson, E. : 1965, *Progress in Oceanography* 3, pp. 221-252.
24. Pastouret, L., Chamley, H., Delibrias, G., Duplessy, J.C., and Thiede, J. : 1978, *Oceanol. Acta* 1, pp. 217-231.

25. Peng, T.-H., Broecker, W.S., Kipphut, G., and Shackleton, N.: 1977, in : "The Fate of Fossil Fuel CO<sub>2</sub> in the Oceans", N.R. Andersen and A. Malahoff (Eds), Plenum Publ. Corp., New York, pp. 355-373.
26. Prell, W.L. : 1982, in : "Initial Reports of the Deep Sea Drilling Project", W.L. Prell and J.V. Gardner (Eds), LXVIII, U.S. Government Printing Office, Washington, pp. 455-464.
27. Prell, W.L., Imbrie, J., Morley, J.J., Pisias, N.G., Shackleton, N.J., and Streeter, H. : 1983, "Graphic correlation of oxygen isotope records : application to the late Quaternary", MS in prep.
28. Shackleton, N.J. : 1967, Nature (Lond.) 215, pp. 15-17.
29. Shackleton, N.J. : 1969, Proc. Roy. Soc. Lond. B 174, pp. 135-154.
30. Shackleton, N.J. : 1977, Phil. Trans. Roy. Soc. Lond. B 280, pp. 169-182.
31. Mesolella, D.J., Matthews, R.K., Broecker, W.S., and Thurber, D.L. : 1969, J. Geol. 77, pp. 250-274.  
Shackleton, N.J., and Matthews, R.K. : 1977, Nature (Lond.) 6, pp. 445-450.
32. Shackleton, N.J., and Opdyke, N.D. : 1973, Quaternary Research 3, pp. 39-55.
33. Shackleton, N.J., and Opdyke, N.D. : 1976, in : "Investigation of late Quaternary Paleoceanography and Paleoclimatology", R.M. Cline and J.D. Hays (Eds), Geol. Soc. Amer. Mem. 145, pp. 449-464.
34. Stuiver, M., Quay, P.D., and Ostlund, H.G. : 1983, Science 219, pp. 849-851.
35. Tse, F.S., Morse, I.E., and Hinkle, R.T. : 1978, "Mechanical vibrations theory and applications", 2nd ed., Allyn and Bacon, Boston.
36. Thierstein, H.R., Geitzenauer, K.R., Molfino, B., and Shackleton, N.J. : 1977, Geology 5, pp. 400-414.
37. Thompson, P.R., and Sciarrillo, J.R. : 1978, Nature (Lond.) 275, pp. 29-33.
38. Weertman, J. : 1964, J. Glaciology 38, pp. 145-158.
39. See (15) for historical reviews of the astronomical theory.
40. Bjore Kullenberg invented a piston-coring device that was used by scientists of the Swedish Deep-Sea Expedition (1947-48) to recover long sections of deep-sea sediment.
41. In a later paper, we will document the phase characteristics of the five individual cores, which are not significantly different from those of the stacked record.
42. Unpublished data of Alan Mix, Lamont-Doherty Geological Observatory.
43. Unpublished data of Warren Prell, Brown University.
44. Mankinen and Dalrymple (20) base their estimate of the B/M reversal on 23 K-Ar dates, and their estimate of the Top Jaramillo reversal on 13 K-Ar dates. The confidence

intervals given in Table 5 are pooled estimates of error made by the authors after discussing the matter with G. Brent Dalrymple.

45. In V22-174 and DSDP502b, the B/M reversal occurs at depths of 1405 cm and 1626 cm, respectively. In V28-238, it occurs at 1201 cm. As noted in Table 6, 30 cm must be subtracted from this depth to be consistent with our tuning procedures.